

Split and Knit: 3D Fingerprint Capture with a Single Camera

Apoorva Srivastava

Biometrics and Secure ID Lab, CVIT, IIIT Hyderabad
India

CCS CONCEPTS

- Computing methodologies → Computer vision; 3D imaging.

KEYWORDS

3D Fingerprint Reconstruction, Photometric Stereo

ACM Reference Format:

Apoorva Srivastava and Anoop M. Namboodiri. 2022. Split and Knit: 3D Fingerprint Capture with a Single Camera. In *Proceedings of the Thirteenth Indian Conference on Computer Vision, Graphics and Image Processing (ICVGIP'22), December 8–10, 2022, Gandhinagar, India*. ACM, New York, NY, USA, Article 18, 4 pages. <https://doi.org/10.1145/3571600.3571618>

1 3D FINGERPRINT ACQUISITION SETUP DETAILS

To design a photometric stereo-based fingerprint scanner, the main steps involved were (*i*) Deciding the parameters of the Setup, LEDs, and Camera, (*ii*) 3D printing the setup, (*iii*) Calibrating the camera and the Lighting direction of LEDs. We describe each of the steps in detail in the following sub-sections.

1.1 Deciding the parameters of the Setup, LED, and Camera

For determining the exact locations of LEDs, the height of the LED and camera, the camera's resolution, the LED's brightness, and the LED's angular orientation, we simulated the photometric stereo on Blender [Community 2018]. We reconstructed the 3D finger using photometric stereo for a synthetic 3D finger model. The best parameters were the ones that minimized the Hausdorff distance [Kraft 2020] between the original 3D finger point cloud and the output 3D finger obtained via photometric stereo. We decided the height of the LEDs and camera to be 14 cm. It also satisfied the basic assumptions of photometric stereo [Woodham 1992], that is, the direct component of LED light does not reach the camera as both were placed on the same plane. LEDs were placed in a circle of radius 5.25 cm at 20° towards the circle's center. We chose Raspberry Pi NoIR Camera Module v2, which has an 8 megapixel SonyIMX219 image sensor custom-designed add-on board for Raspberry Pi, with a fixed focus lens. The chosen camera can capture both the NIR and visible light spectrum. The LEDs and the camera were controlled using a Raspberry pi 4B model, and a separate PCB was designed to power the LED circuit.

Permission to make digital or hard copies of all or part of this work for personal or classroom use is granted without fee provided that copies are not made or distributed for profit or commercial advantage and that copies bear this notice and the full citation on the first page. Copyrights for components of this work owned by others than the author(s) must be honored. Abstracting with credit is permitted. To copy otherwise, or republish, to post on servers or to redistribute to lists, requires prior specific permission and/or a fee. Request permissions from permissions@acm.org.

ICVGIP'22, December 8–10, 2022, Gandhinagar, India

© 2022 Copyright held by the owner/author(s). Publication rights licensed to ACM.
ACM ISBN 978-1-4503-9822-0/22/12...\$15.00
<https://doi.org/10.1145/3571600.3571618>

Anoop M. Namboodiri

Biometrics and Secure ID Lab, CVIT, IIIT Hyderabad
India

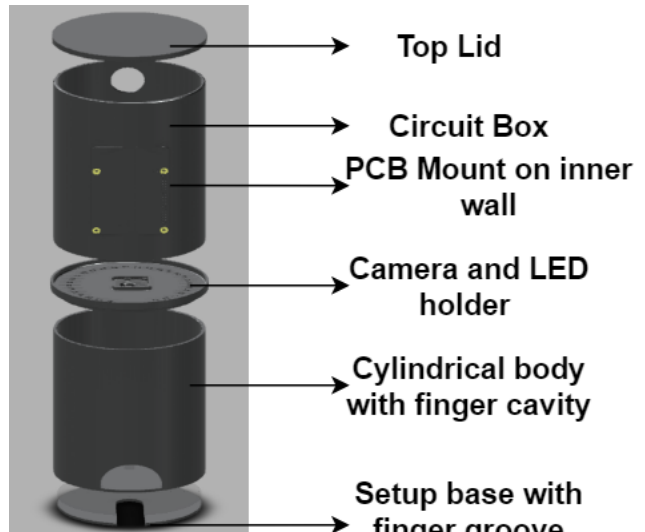


Figure 1: 3D Printed fingerprint capture setup

1.2 3D printing the setup

The setup was 3D printed as different parts capable of being plugged together. The setup components are shown in Figure 1. There are four major parts: i) The setup floor has a fixed groove for the finger to get support and restrict movement. The color of the floor is kept black for easier separation of the finger from the background based on chromaticity. ii) Cylindrical box with a height of 14 cm to provide the space between LED and finger and to prevent outside illumination. It has a cavity for inserting the finger into the setup. iii) Cylinder's roof has small holes for the LEDs in the periphery and a rectangular slot for the camera in the center. It prevents any direct component of the LED light from reaching the camera, a fundamental assumption in photometric stereo [Woodham 1992]. iv) Circuit box is placed at the top of the roof of the cylinder to confine the PCBs for LED, raspberry pi, and camera. The PCBs are mounted on the inner wall of the circuit box using screws. Above the circuit box, there is a lid to prevent outside illumination.

1.3 Calibrating the Camera and Lighting Directions

The camera was calibrated using Zhang's method [Zhang 2000] by clicking focused checkerboard images. The lighting directions were calibrated using a simple conical structure with a height of 3.5 cm and a diameter of 1 cm, as mentioned in [Kumar 2018]. The method involved clicking images of the conical object under different lights and determining the direction of lights by tracing the tip of the shadow of the conical object along each lighting direction. For a

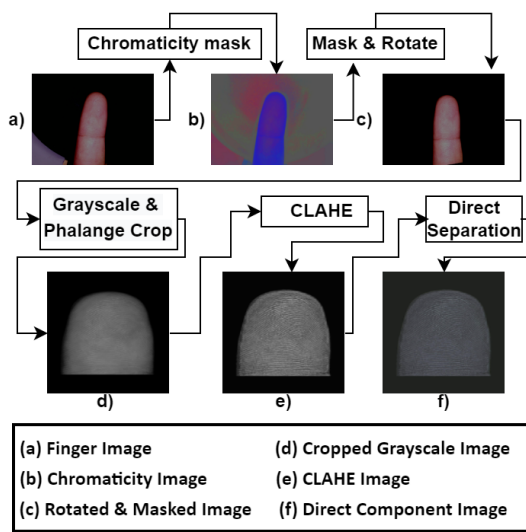


Figure 2: (a)-(d) Preprocessing steps to obtain the grayscale image of the first phalange segmented at a zero-degree yaw angle, (e)-(f) Steps to reduce the non-lambertian nature of the finger image.

given lighting direction, the tip of the shadow and the center of the conical structure forms the 2D projection of the ray of light coming toward the calibration object. Finding the intersection of this ray with the LED circle gives the exact location of the LED. We obtained the rays for all the lighting directions and found their intersection with the LED circle to determine the LED location over multiple observations.

2 PRE-PROCESSING STEPS

As mentioned in section 2.3.2 in the main paper, figure 2 displays the preprocessing steps. The first step is to segment the finger from the background using the finger's chromaticity image [Shen et al. 2008; Tan and Ikeuchi 2005]. Then, by detecting the angular orientation of the mask's longitudinal axis, the yaw angle is made zero for all the fingers. The mask's longitudinal axis is determined by finding the midpoint of each row of the mask image and fitting a line on the set of midpoints obtained.

The sub-surface scattering creates an irregular red hue on the finger surface, acting as noise. The conversion from RGB to grayscale suppresses the effect of color in the white light images. Afterward, the phalange segmentation is performed by detecting the first vein of the finger and cropping out the phalange. For detecting the first vein of the finger, multiple image processing steps of gaussian blurring and contrast enhancement were applied to obtain the location of the first vein as the location of the most dominant horizontal edge. The finger was cropped from the obtained location to obtain the first phalange. The final output of the preprocessing steps is 1528x936 resolution cropped images with the first phalange of a finger at zero degrees yaw angle. Figure 2 (e) shows the enhancement obtained in the fingerprint after applying CLAHE over the 64x64 neighborhood windows of the grayscale fingerprint images.

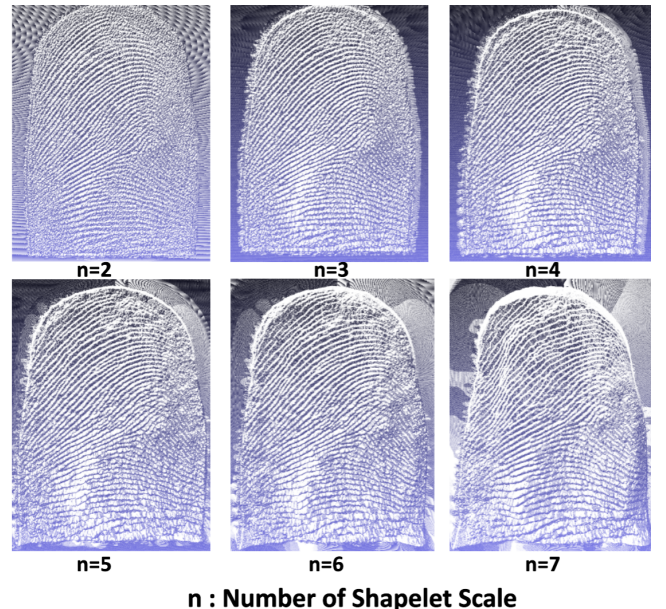


Figure 3: With an increase in the number of shapelet scale (n), the low-frequency information increases, which distorts the global finger shape. We found the initial 3 shapelet scales most suitable to extract the ridge-valley point cloud, as they provided the best matching performance.

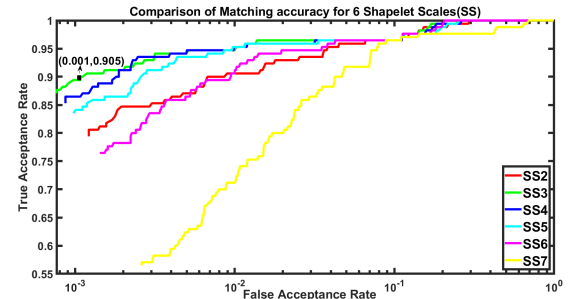


Figure 4: ROC curves for matching ridge-valley point cloud for fingers captured over two sessions with different shapelet scales varying from 2 to 7. The highest 90.5% GAR @ 0.001 FAR is obtained for shapelet Scale 3(SS3). Hence, using 3 shapelet scales, we obtain the highest quality ridge-valley pattern.

3 ANALYSIS OF SHAPELET SCALE

As mentioned in section 2.3.5 of the main paper, shapelet scales can be used to reconstruct point clouds from the surface normals obtained from the photometric stereo. As the number of shapelet scales increases, the lower frequency component increases in the reconstructed point cloud. To get the ridge-valley pattern extracted from the reconstructed finger structure, we need only the high-frequency component of the structure. To determine the correct number of shapelet scales for extracting the ridge-valley pattern, we

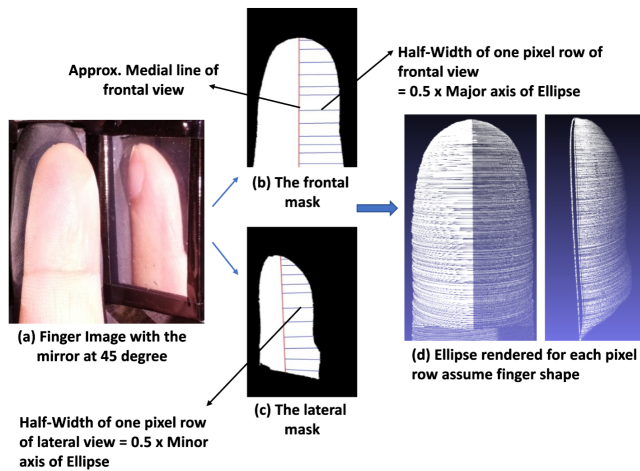


Figure 5: Alternative method to obtain finger shape with a single image obtained using a mirror, camera, and parametric modeling of the finger with ellipses. This method does not require photometric stereo and IR illumination.

performed a 6 ridge-valley point cloud matching experiment for 170 fingers recorded over 2 sessions. Each of the six experiments had a different shapelet scale varying from 2 to 7. As shown in Figure 4, the highest 90.5%GAR @ 0.001FAR is obtained for shapelet scale 3. It shows that the initial 3 shapelet scales produce the highest quality ridge-valley pattern among all the shapelet scales. Hence, for the Split-and-Knit algorithm, we fixed the shapelet scale to 3. Figure 3 also shows a visual representation that as the shapelet scale increases from $n = 2$ to $n = 7$, there is an increase in low-frequency shape information, distorting the overall finger shape.

4 RECONSTRUCTION OF FINGER SHAPE USING A CAMERA, MIRROR AND A SINGLE IMAGE

As mentioned in section 2.4 in the main paper, we propose a novel method to obtain the finger shape by a single image without photometric stereo and IR illumination requirements. We use a mirror and a camera for this method. Figure 5 elaborates the steps for the same. A mirror is equivalent to a virtual camera, but there will be a single camera in practice. We keep the mirror at 45° tilt beside the finger. It helps the camera observe the occluded side finger in the orthographic view. We mask the frontal and lateral views separately. For each view, we obtain the approximate medial line for the finger. Based on this medial line, we calculate the half-width of the finger for each pixel row in each view. Let us suppose the two views have N corresponding pixel rows. We model an ellipse for a given pixel row with the frontal view half-width and the lateral view half-width as half of the major and minor axis, respectively. Hence, we obtain the overall finger shape by rendering the ellipses for each N -pixel row. Further, we cut the ellipses by half along the minor axis to resemble the finger phalange.

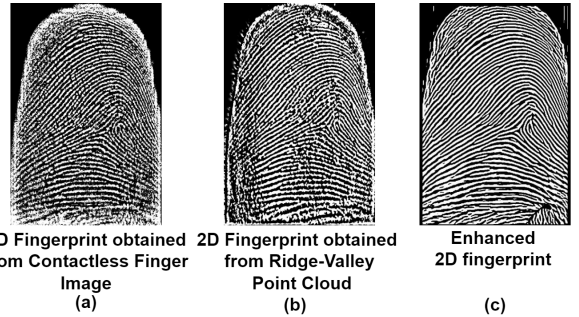


Figure 6: 2D fingerprints obtained from (a) Contactless finger image, and (b) Ridge-Valley range image (c) Enhanced 2D fingerprint. The similarity between a) and b) proves the high-quality ridge-valley point cloud reconstruction. (c) The enhanced fingerprint assures compatibility with 2D fingerprint-matching algorithms.

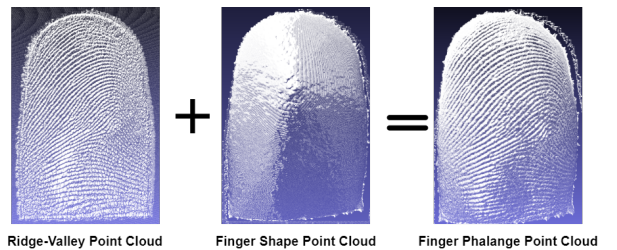


Figure 7: The figure shows the pixel-wise addition of ridge-valley point cloud with finger shape point cloud to obtain the finger phalange point cloud

5 3D TO 2D CONVERSION

In this experiment, we tried to prove the high quality of the ridge-valley point cloud by visualizing the ridge-valley point cloud as a range image. Hence, we obtain the 2D fingerprint in a novel way directly from the range image of the ridge-valley point clouds without any image processing on the point cloud. The traditional method to obtain 2D fingerprints from contactless finger images is by following the enhancement and scaling methods depicted in [Lin and Kumar 2018; Liu et al. 2016]. The 2D fingerprint obtained from visualizing the ridge-valley range image appears similar to the 2D fingerprint obtained by processing the contactless fingerprint, as shown in Fig 6. It again proves the excellent quality of the 3D reconstruction of the ridge-valley point cloud by SnK. Further, we obtained the enhanced fingerprint using Gabor filter-based enhancement. Also, obtaining the 2D fingerprints makes the system use the Split-and-Knit algorithm(SnK) compatible with 2D fingerprint matching algorithms.

REFERENCES

- Blender Online Community. 2018. *Blender - a 3D modelling and rendering package*. Blender Foundation, Stichting Blender Foundation, Amsterdam. <http://www.blender.org>
- Daniel Kraft. 2020. Computing the Hausdorff Distance of Two Sets from Their Distance Functions. *International Journal of Computational Geometry and Applications* 30, 01

- (mar 2020), 19–49. <https://doi.org/10.1142/s0218195920500028>
- Ajay Kumar. 2018. *Contactless 3D Fingerprint Identification*. Edition 1, Springer Cham.
- Chenhai Lin and Ajay Kumar. 2018. Matching Contactless and Contact-Based Conventional Fingerprint Images for Biometrics Identification. *IEEE Transactions on Image Processing* 27, 4 (2018), 2008–2021. <https://doi.org/10.1109/TIP.2017.2788866>
- Xinwei Liu, Marius Pedersen, Christophe Charrier, Faouzi Alaya Cheikh, and Patrick Bours. 2016. An improved 3-step contactless fingerprint image enhancement approach for minutiae detection. In *2016 6th European Workshop on Visual Information Processing (EUVIP)*, 1–6. <https://doi.org/10.1109/EUVIP.2016.7764594>
- Hui-Liang Shen, Hong-Gang Zhang, Si-Jie Shao, and John H. Xin. 2008. Chromaticity-based separation of reflection components in a single image. *Pattern Recognition* 41, 8 (2008), 2461–2469. <https://doi.org/10.1016/j.patcog.2008.01.026>
- R.T. Tan and K. Ikeuchi. 2005. Separating reflection components of textured surfaces using a single image. *IEEE Transactions on Pattern Analysis and Machine Intelligence* 27, 2 (2005), 178–193. <https://doi.org/10.1109/TPAMI.2005.36>
- Robert Woodham. 1992. Photometric Method for Determining Surface Orientation from Multiple Images. *Optical Engineering* 19 (01 1992). <https://doi.org/10.1117/12.7972479>
- Z. Zhang. 2000. A flexible new technique for camera calibration. *IEEE Transactions on Pattern Analysis and Machine Intelligence* 22, 11 (2000), 1330–1334. <https://doi.org/10.1109/34.888718>